P H Y S I C A L   R E V I E W   L E T T E R S

Momentum Dependence of the Electron-Phonon Coupling and Self-Energy Effects in Superconducting YBa$_2$Cu$_3$O$_7$ within the Local Density Approximation

Rolf Heid,[1] Klaus-Peter Bohnen,[1] Roland Zeyher,[2] and Dirk Manske[2]

[1]*Forschungszentrum Karlsruhe, Institut für Festkörperphysik, P. O. Box 3640, D-76021 Karlsruhe, Germany*
[2]*Max-Planck-Institut für Festkörperforschung, Heisenbergstrasse 1, D-70569 Stuttgart, Germany*

Using the local density approximation and a realistic phonon spectrum we determine the momentum and frequency dependence of $\alpha^2 F(\mathbf{k}, \omega)$ in YBa$_2$Cu$_3$O$_7$ for the bonding, antibonding, and chain band. The resulting self-energy Σ is rather small near the Fermi surface. For instance, for the antibonding band the maximum of ReΣ as a function of frequency is about 7 meV at the nodal point in the normal state and the ratio of bare and renormalized Fermi velocities is 1.18. These values are a factor of 3–5 too small compared to the experiment showing that only a small part of Σ can be attributed to phonons. Furthermore, the frequency dependence of the renormalization factor $Z(\mathbf{k}, \omega)$ is smooth and has no anomalies at the observed kink frequencies which means that phonons cannot produce well-pronounced kinks in stoichiometric YBa$_2$Cu$_3$O$_7$, at least, within the local density approximation.

Angle resolved photoemission (ARPES) experiments in high-T_c cuprates show that electrons near the Fermi surface interact strongly with bosonic excitations causing a kink in their dispersion at rather well-defined energies [1–3]. The most popular candidates for the bosonic excitations are spin fluctuations [4] and phonons [2]. Plausible arguments have been put forward for either of the two choices, but no consensus has been reached up to now on which of these two possibilities actually is realized in the cuprates. Recently, an explanation of these effects entirely in terms of phonons has been proposed identifying the 40 and 70 meV kink energies with the buckling and the breathing phonon modes [5]. It was also argued that the electron-phonon (ep) coupling in these systems is strongly anisotropic with respect to momenta and phonon branches and that the coupling to the breathing and the buckling phonon modes takes place at different points in the Brillouin zone [5], which would provide a natural explanation of several observations.

Assuming that the local density approximation (LDA) for stoichiometric YBa$_2$Cu$_3$O$_7$ represents a reasonable first approximation for the electron-phonon coupling in doped cuprates it is the aim of this Letter to find out whether an explanation of the kink phenomenon entirely in terms of phonons is possible. To this end we generalize previous calculations [6] for the Eliashberg function where both momenta were averaged over the Fermi surface to the case where the average is done only with respect to one momentum. Multiplying with $2/\omega$ and considering a general electronic band ν the resulting function $\lambda_\nu(\mathbf{k}, \omega)$ can be used to study the anisotropy of the electron-phonon interaction as a function of the momentum and frequency using realistic phonon branches determined from first principles. Our approach omits possible effects due to strong electronic correlations beyond the LDA, a problem which presently is unsettled. This shortcoming seems not to be

very serious for our work and conclusions because several calculations suggest [7,8] that strong electronic correlations tend to decrease rather to increase the ep interaction in $\mathbf{q}$-integrated quantities such as the self-energy.

The momentum and frequency dependent coupling function $\lambda_\nu(\mathbf{k}, \omega)$ is defined by [9]

$$\lambda_\nu(\mathbf{k}, \omega) = \frac{2}{\omega} \sum_{\mathbf{q}, j, \mu} |g_j(\mathbf{k}\nu, \mathbf{k}+\mathbf{q}\mu)|^2 \cdot \delta(\omega - \omega_{\mathbf{q}j}) \delta(\epsilon_{\mathbf{k}+\mathbf{q}\mu}). \tag{1}$$

$g_j(\mathbf{k}\nu, \mathbf{k}+\mathbf{q}\mu)$ denotes the amplitude for a transition from the electronic state with momentum $\mathbf{k}$ and band index ν to the state with momentum $\mathbf{k}+\mathbf{q}$ and band index μ creating (annihilating) a phonon with branch label j and momentum $\mathbf{q}$ ($-\mathbf{q}$). $\omega_{\mathbf{q}j}$ and $\epsilon_{\mathbf{k}\nu}$ are the eigenenergies of the phonons and electrons, respectively; the latter are measured relative to the chemical potential. Additional calculations suggest that λ can be considered to be diagonal in the band indices. A direct evaluation of Eq. (1) is difficult because high numerical costs restricted the calculation of the matrix elements g to rather coarse $\mathbf{q}$ meshes. Large fluctuations due to a small number of terms in Eq. (1) can be avoided, however, by introducing Fermi-surface harmonics [10]. In this approach, the $\mathbf{k}$ dependence of $\lambda_\nu(\mathbf{k}, \omega)$ is expanded in a basis set of functions W formed by products of an even power of electron velocities $v_\alpha(\mathbf{k}\nu) = \partial \epsilon_{\mathbf{k}\nu}/\partial \mathbf{k}_\alpha$ where α is a Cartesian index. We explicitly write

$$\lambda_\nu(\mathbf{k}, \omega) = \sum_{\mathbf{n}} W(\mathbf{n}, \mathbf{k}\nu)\Lambda_\nu(\mathbf{n}, \omega), \tag{2}$$

$$W(\mathbf{n}, \mathbf{k}\nu) = v_x^{2n_x}(\mathbf{k}\nu) v_y^{2n_y}(\mathbf{k}\nu) v_z^{2n_z}(\mathbf{k}\nu), \tag{3}$$

with $\mathbf{n} = (n_x, n_y, n_z)$. Defining the Fermi-surface average

of a variable $X(\mathbf{k})$ by

$$\langle\langle X\rangle\rangle_\nu = \sum_{\mathbf{k}}\delta(\epsilon_{\mathbf{k}\nu})X(\mathbf{k})\Big/\sum_{\mathbf{k}}\delta(\epsilon_{\mathbf{k}\nu}),\qquad(4)$$

we define

$$\lambda_\nu(\mathbf{n},\omega)=\langle\langle W(\mathbf{n},\mathbf{k}\nu)\lambda_\nu(\mathbf{k},\omega)\rangle\rangle_\nu.\qquad(5)$$

Inserting Eq. (2) into Eq. (5) one can solve for the coefficients $\Lambda_\nu(\mathbf{n},\omega)$, and one obtains

$$\lambda_\nu(\mathbf{k},\omega)=\sum_{\mathbf{n}}W(\mathbf{n},\mathbf{k}\nu)\sum_{\mathbf{m}}S_\nu^{-1}(\mathbf{n},\mathbf{m})\lambda_\nu(\mathbf{m},\omega),\qquad(6)$$

with

$$S_\nu(\mathbf{n},\mathbf{m})=\langle\langle W(\mathbf{n},\mathbf{k}\nu)W(\mathbf{m},\mathbf{k}\nu)\rangle\rangle_\nu.$$

Calculation of the quantities $\lambda_\nu(\mathbf{n},\omega)$ involves Fermi-surface averages of the squared matrix elements g weighted by the basis functions W, which can be easily performed within LDA. Once $\lambda_\nu(\mathbf{n},\omega)$ are known, $\lambda_\nu(\mathbf{k},\omega)$ can be obtained from Eq. (6). Typically 10 functions $W(\mathbf{n},\mathbf{k}\nu)$ were used in the following calculations. The sum over electron momenta in Eq. (4) was carried out on a dense $36\times36\times4$ mesh. For the momenta $\mathbf{q}$ we used a $12\times12\times4$ mesh. δ functions in Eqs. (1) and (4) involving electronic energies were approximated by a Gaussian with a width of 0.2 eV. Additional calculations using more basis functions and a smaller width for the Gaussian showed that our results are reasonably stable against larger basis sets or a refined representation of the δ functions.

Figure 1 shows $\lambda_\nu(\mathbf{k},\omega)$ integrated over the frequency from 0 to 50 meV (left column) and from 50 to 80 meV (right column). The diagrams in the first row refer to the bonding, those in the second row to the antibonding, and those in the third row to the chain band. The latter two are partly hybridized in the $(0.5, 0)$ direction. The diagrams were calculated for $k_z = 0.125$, but the corresponding ones for $k_z = 0.375$ look very similar; i.e., the diagrams are practically independent of the momentum perpendicular to the planes. The thick and thin black lines correspond to lines with $\epsilon_{\mathbf{k}\nu} = 0$ and ±0.2 eV, respectively. As the above numerical procedure incorporates only quantities in the vicinity of the Fermi surface, the calculated values for $\lambda_\nu(\mathbf{k},\omega)$ are reliable in the region between the thin black lines whereas larger errors may be expected for momenta far away from the Fermi surface.

The diagrams in the first row of Fig. 1 show that the coupling functions associated with the bonding band have approximately tetragonal symmetry but that they vary along the Fermi line: Their minima and maxima occur at the nodal and antinodal points, respectively, leading to a variation of about a factor of 1.5 and 1.3 for phonons below and above 50 meV, respectively. Whereas a momentum-dependent λ would be in line with the scenario of Ref. [5] there are serious discrepancies: The coupling to high-frequency phonons, for instance to the breathing and half-breathing modes, should show a maximum in nodal
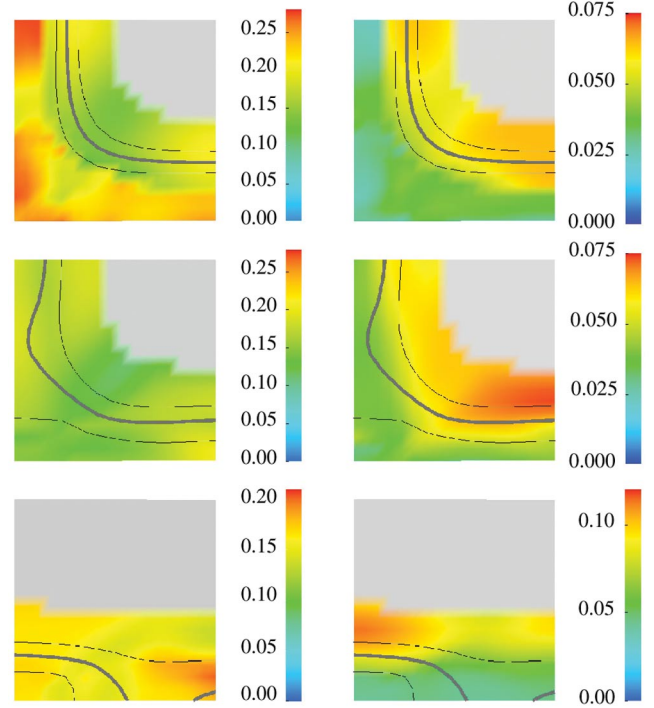

FIG. 1 (color). Coupling function $\lambda_\nu(\mathbf{k},\omega)$ integrated over ω between 0 and 50 meV (left diagrams) and ω larger than 50 meV (right diagrams). Shown are xy cuts through the irreducible Brillouin zone ($0 \le k_x, k_y \le 0.5$) for $k_z = 0.125$. The upper plots refer to the bonding, the middle ones to the antibonding, and the lower ones to the chain band. The latter two are hybridized in the $(0.5, 0)$ direction. The gray areas represent states with energies far away (≥0.8 eV) from the Fermi energy.

direction whereas we find that it has there a minimum similar as in the case of low-frequency modes. In other words, the coupling to high- and low-frequency modes at the nodal and antinodal points is very similar which means that electronic self-energies due to phonons at these two points will not select predominantly low- or predominantly high-frequency phonons. Furthermore, the variation of λ along the Fermi line is rather small in our case, i.e., λ cannot be considered to be very anisotropic. The diagrams in the second row of Fig. 1 describe λ associated with the antibonding band, except for a part close to $(0.5, 0)$, where an exchange of character with the chain band occurs (lower diagrams of Fig. 1). However, the antibonding states in the antinodal direction along $k_y \approx 0.5$ and in the nodal direction are not affected by this hybridization. The momentum dependence of λ associated with the antibonding band resembles that of the bonding band. The coupling of electrons near the Fermi line to low- and to high-frequency phonons is again rather similar as a function of $\mathbf{k}$; the absolute values for λ are roughly larger by a factor of 3 for low- than for high-frequency phonons, similar to the case of the bonding band. The same trend is found for the chain band, with an anisotropy of the order of 2 or smaller. Using a $4\times4\times2$ mesh for $\mathbf{q}$ yields qualitatively similar results for λ as the $12\times12\times4$ mesh. Quantitatively, the

difference between the bond and antibonding bands as well as their anisotropies are more pronounced in this case, in particular, for the bonding band. The present inversion procedure leads in this case also to unphysical small negative values for λ in a small region away from the Fermi line for the bonding band which does not occur for the employed finer $12 \times 12 \times 4$ mesh.

The following results refer to the antibonding band; thus, from now on we drop the band index ν. Figure 2 shows frequency-resolved coupling functions $\lambda(\mathbf{k}, \omega)$ for momenta near the Fermi line in nodal (upper diagram) and antinodal (lower diagram) directions. The solid lines correspond to $k_z = 0.375$, the dotted lines to $k_z = 0.125$. The differences between the solid and dotted lines are very small reflecting the very small k_z dependence of λ. The spectra are very broad and extend over the entire one-phonon range. It is evident that models which use only one or a few selected phonons are not able to represent adequately the phonon spectrum.

The imaginary part of the retarded electronic self-energy due to phonons can be written as [9]

$$\mathrm{Im}\Sigma(\mathbf{k}, \omega) = -\frac{\pi}{2} \int_0^\infty du\, u\lambda(\mathbf{k}, u)[2b(u) + f(u - \omega) + f(u + \omega)]. \tag{7}$$
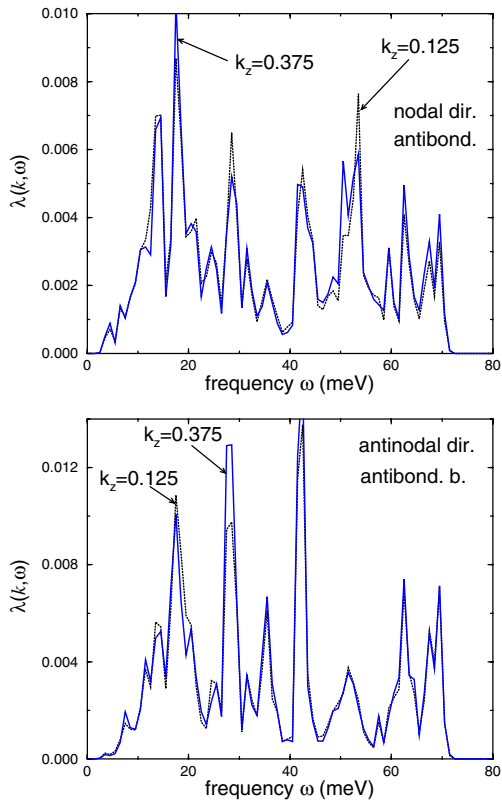

FIG. 2 (color online).   Momentum and frequency-resolved coupling function $\lambda(\mathbf{k}, \omega)$ in 1/meV of the antibonding band near the Fermi surface in the nodal (upper diagram) and the antinodal (lower diagram) direction. Solid and dotted lines correspond to $k_z = 0.375$ and 0.125, respectively.

Here, b and f denote the Bose and the Fermi functions, respectively, and we assumed the self-energy to be diagonal in the band index. The corresponding real part of Σ was obtained by a Kramers-Kronig transformation using a cut-off of 1 eV. Figure 3 shows the calculated self-energy near the nodal and antinodal Fermi points using the coupling functions of Fig. 2. The negative imaginary part of Σ increases monotonically over the whole phonon spectrum and then approaches a constant. The negative real part increases first, passes through a maximum roughly in the middle of the phonon spectrum, and then decreases monotonically. Both the real and imaginary parts of Σ exhibit small oscillations as a function of frequency which reflect the many maxima in $\lambda(\mathbf{k}, \omega)$ and the complexity of the phonon spectrum. At elevated temperatures (for instance, at $T = 9$ meV) these oscillations vanish; the maximum in $\mathrm{Re}\Sigma$ becomes somewhat smaller and $\mathrm{Im}\Sigma$ finite at zero frequency, but otherwise there is no substantial change in Σ. Figure 3 also illustrates the small anisotropy of Σ: In the antinodal direction Σ is only slightly larger compared to the nodal direction while the position of the maximum of $\mathrm{Re}\Sigma$ is approximately the same. For the nodal direction experimental values for the maximum of $\mathrm{Re}\Sigma$ are 20–40 meV [3,11] whereas we have only about 7 meV at $T = 9$ meV.

Figure 4 shows the frequency dependence of the renormalization function Z, defined by $Z(\mathbf{k}, \omega) = 1 - \mathrm{Re}\Sigma(\mathbf{k}, \omega)/\omega$, near the nodal and antinodal Fermi points. At zero frequency Z is equal to $1 + \lambda(\mathbf{k})$ where $\lambda(\mathbf{k})$ is the frequency-integrated, dimensionless coupling constant depending still on the momentum. This coupling constant is about 0.18 and 0.22 at the nodal and antinodal points, respectively, illustrating again the smallness of the electron-phonon coupling. With increasing frequency Z increases first slightly, passes through a maximum and then approaches unity beyond the end of the one-phonon spectrum. Superimposed on this general behavior are many
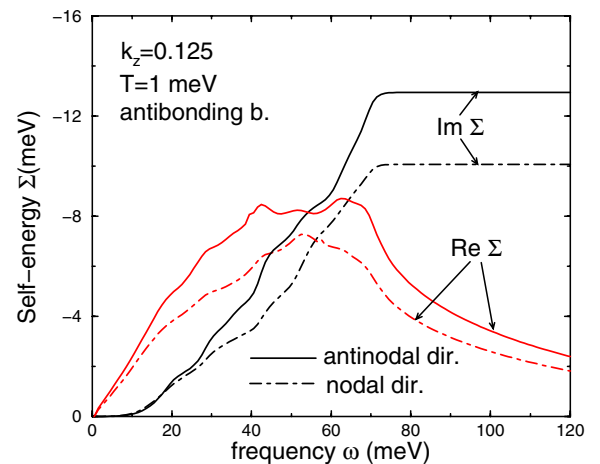

FIG. 3 (color online).   Real and imaginary parts of the self-energy Σ of the antibonding band near the Fermi points along the nodal and antinodal directions at the temperature $T = 1$ meV.
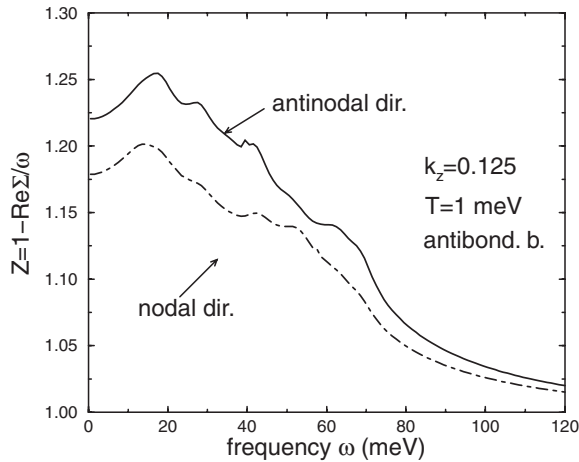
FIG. 4. Renormalization function $Z(\mathbf{k}, \omega)$ of the antibonding band near the Fermi points in nodal and antinodal directions for $k_z = 0.125$ at the temperature $T = 1$ meV.
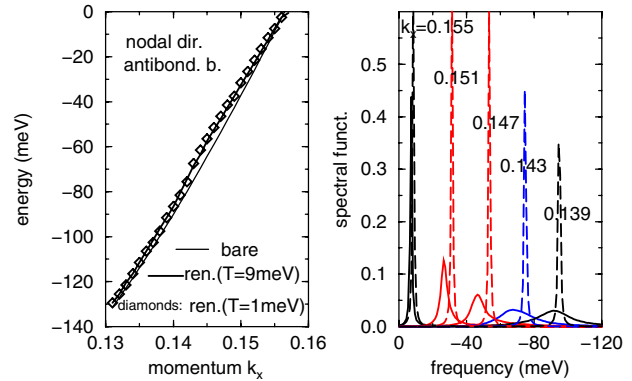

FIG. 5 (color online). Left: Electronic dispersion; right: spectral function of the antibonding band for different momenta $k_x = k_y$ along the nodal direction using $T = 1$ meV and $k_z = 0.125$.

small oscillations which reflect the numerous density peaks in Fig. 2 and which vanish already at $T = 9$ meV. If, as in our case, the imaginary part of Σ is rather small, the dispersion of the electrons is given by the equation $\omega = \epsilon_{\mathbf{k}}/Z(\mathbf{k}, \omega)$ which for small Σ's has the solution $\omega = \epsilon_{\mathbf{k}}/Z(\mathbf{k}, \epsilon_{\mathbf{k}})$. A kink in the dispersion is generated if Z changes from a large to a small value in a narrow frequency interval. This happens, for instance, in a model with one single optical phonon; see Fig. 2 of Ref. [12]. However, for our realistic phonon spectrum and coupling functions this does not occur according to Fig. 4, so there will be no well-pronounced kink feature in the electronic dispersion. There seems to be a general consensus that ARPES data for the nodal and antinodal directions yield kink energies of about 70 and 40 meV, respectively. It is clear that these energies do not represent any characteristic energies in the frequency dependence of Z in Fig. 4.

Finally, the left diagram in Fig. 5 illustrates the weakness and smoothness of the renormalization of the dispersion of the antibonding band in the nodal direction and also its weak dependence on temperature. The ratio of asymptotic slopes at small and large frequencies is about 1.18 which is much smaller than typical experimental values of about 2 in optimally doped cuprates [2,3,13]. The right diagram in Fig. 5 shows spectral functions of the antibonding band along the nodal direction for five different momenta $k_x = k_y$. Unlike in the case of one optical phonon coupled strongly to electrons, discussed in Ref. [12], the solid lines show always only one peak which departs and then returns very smoothly from the noninteracting peak with decreasing energy.

Based on the above LDA results our main conclusions are: (a) the coupling function $\lambda(\mathbf{k}, \omega)$ shows as a function of $\mathbf{k}$ a minimum at the nodal and a maximum at the antinodal Fermi point rather independently of the involved phonon modes. The resulting anisotropy in $\mathbf{k}$ is rather moderate both for the bonding and the antibonding band; (b) it is important to keep a realistic phonon spectrum and not only one or two phonon branches because the ω dependence of λ is mainly determined by phonon densities where, for instance, the breathing or the buckling mode do not play any distinguished role; (c) the frequency-integrated coupling function $\lambda(\mathbf{k})$ varies between 0.18 and 0.22 along the Fermi surface. Because of these rather small values the phonon-induced electronic self-energies along the nodal direction are too small by about a factor of 3–5 to account for the self-energies deduced from ARPES experiments and for the observed slope changes in the electronic dispersion, at least, within the LDA.

The authors thank T. P. Devereaux for discussions and clarifications concerning, in particular, the correct definition of λ in a multiband superconductor.

[1] P. V. Bogdanov *et al.*, Phys. Rev. Lett. **85,** 2581 (2000).
[2] A. Lanzara *et al.*, Nature (London) **412,** 510 (2001).
[3] A. D. Gromko *et al.*, Phys. Rev. B **68,** 174520 (2003).
[4] D. Manske, I. Eremin, and K.-H. Bennemann, Phys. Rev. Lett. **87,** 177005 (2001).
[5] T. P. Devereaux, T. Cuk, Z.-X. Shen, and N. Nagaosa, Phys. Rev. Lett. **93,** 117004 (2004).
[6] K.-P. Bohnen, R. Heid, and M. Krauss, Europhys. Lett. **64,** 104 (2003).
[7] R. Zeyher and M. L. Kulić, Phys. Rev. B **53,** 2850 (1996).
[8] Z. B. Huang, W. Hanke, E. Arrigoni, and D. J. Scalapino, Phys. Rev. B **68,** 220507 (2003).
[9] G. D. Mahan, *Many-Particle Physics* (Plenum Press, New York, 1990).
[10] P. B. Allen, Phys. Rev. B **13,** 1416 (1976).
[11] X. J. Zhou *et al.*, Phys. Rev. Lett. **95,** 117001 (2005).
[12] R. Zeyher and A. Greco, Phys. Rev. B **64,** 140510(R) (2001).
[13] J. D. Koralek *et al.*, Phys. Rev. Lett. **96,** 017005 (2006).